



Assessment of New Adaptive Finite Elements Based on Carrera Unified Formulation for Meshes with Arbitrary Polygons

M. Cinefra¹ · A. Rubino¹

Received: 6 April 2023 / Revised: 11 July 2023 / Accepted: 13 July 2023 / Published online: 8 August 2023
© The Author(s) 2023

Abstract

The meshing technique represents the capability to discretize the domain of interest, to fit the real physical continuum in the best possible way. The most used approach is the finite-element method (FEM), a numerical method to solve partial differential equations. To overcome the classical issues presented by FEM, other models are investigated. The goal is to allow the problem domain to be discretized by elements represented by arbitrary polygons, which can be concave and convex. Moreover, different polynomial consistency is sought within these methods with the possibility to handle non-conforming discretizations, mainly for local refinement and so on. This work aims to present the new adaptive elements, which are finite elements based on Carrera unified formulation, to demonstrate that all the previous capabilities can be done with these new elements, with easy implementation of the relative model. First, a classical patch test is done to investigate the mesh distortion sensitivity. Then, different study cases are presented with more complex meshes combining very distorted concave and convex elements.

Keywords Carrera unified formulation · Virtual element method · Plate finite elements · Beam Finite Elements · Node-dependent kinematics · Non-orthogonal geometry

1 Introduction

The meshing technique represents the capability to discretize the domain of interest, to fit the real physical continuum in the best possible way. In the engineering field, meshing is a crucial milestone in creating the model of the problem to solve, it is the starting point on which the simulation is performed and it is important that it can represent in the more accurate way the analyzed domain. The physical area investigated is not so regular, in general, and the meshing should account for it.

The most used technique is the finite-element method (FEM), which relies on a quite simple mathematical model capable of describing the field under investigation (structural and/or fluid dynamic) up to a certain level of accuracy. This method allows the construction of 2D and 3D regular elements with a prescribed number of nodes each [1]. The main

issues of this method are represented by: the constraint to regular presetting of elements; the difficulties managing different types of elements on the same domain, perhaps with a different number of nodes, therefore, a different approximation; the high computational cost due to the high number of elements used, to adapt when the real domain it is not geometrically regular or when enrichment of the mesh is required, because it is in the area of interest.

To alleviate meshing issues due to FEM, more advanced techniques can be used, resorting to numerical methods that are designed from the very beginning to provide arbitrary order of accuracy on more generally shaped elements. These techniques are based, for instance, on the virtual element method (VEM) or polytopal element method (PEM) [2]. In fact, in contrast to FEM in which elements are typically triangular and quadrilateral in 2D or tetrahedral and hexahedral in 3D, the VEM permits arbitrary two-dimensional polygonal and three-dimensional polyhedral elements [3, 4], having many aspects closely connected with FVM and in particular with mimetic finite differences (MFD) [5]. This allows the problem domain to be discretized by elements represented by arbitrary polygons, which can be concave and convex. Moreover, different polynomial consistency is

✉ M. Cinefra
maria.cinefra@poliba.it

¹ Department of Mechanics, Mathematics and Management, Politecnico di Bari, Via Edoardo Orabona 4, 70126 Bari, Italy

allowed within the method and non-conforming discretizations can be handled, mainly for local refinement and so on, representing the key aspect of this method [6].

The newly proposed adaptive elements, which are finite elements based on Carrera unified formulation (CUF), represent more agile and manageable elements, based on a well-known technique (FEM), easy to implement and can produce the same benefits obtained using VEM. As a matter of fact, the CUF, applied both to 1D and 2D finite elements, provides very accurate 3D-like solutions with much lower computational cost than the classical 3D elements, becoming an important tool for the analysis of structural problems.

Recently, in the framework of CUF, a novel approach called node-dependent kinematics (NDK) has been proposed to further increase the numerical efficiency of the models [7–11]. By relating the kinematic assumptions to the chosen nodes, FE models with variable nodal kinematics can be built conveniently. Naturally, the critical zone with higher order assumptions can be bridged to the less-critical area modeled with adequate lower order theories [12], in such a way the numerical modeling procedure can further be simplified.

The NDK approach, along with the 3D modelling of non-orthogonal geometries, opens the possibility to create elements with a non-conventional number of nodes, with non-conventional geometrical shapes, and with different polynomial approximations along different directions, leading to a certain freedom in constructing proper elements. These elements are formulated considering that the integrals inside the matrices of the governing equations (stiffness and mass matrices), which involves the approximating functions, and the Jacobian matrix of the elements are computed in 3D form, although 1D and 2D CUF models are still employed. In conclusion, 3D elements can be recovered with a non-regular shape that can adapt to the edges of the domain considered or to adjacent portions which share one or more sides, when the geometrical constraints or the kinematic behaviour require that.

The paper is organized as follows: an introduction is presented in Sect. 1; the 1D and 2D models based on CUF are briefly recalled in Sect. 2; the derivation of governing equations from the Principle of Virtual Displacements by using both the finite-element method and the CUF is presented in Sect. 3, where also the present approach is explained in the framework of NDK technique along with the 3D modelling; Sect. 4 contains the results obtained by the static and modal analysis of some useful study cases that demonstrate the capabilities of the present elements; finally, Sect. 5 summarises the conclusions of this work.

2 Carrera Unified Formulation: 1D and 2D Models

The CUF (see [13, 14]) describes the kinematic field in a unified manner that will be then exploited to derive the governing equations in a compact way, which are easy to implement unlike the VEM. This compact form represents an huge advantage with respect to classical theories, that have several limitations (as explained in many previous works related to CUF). The main of those limitations is that the kinematics should be theoretically enriched with an infinite number of terms (see Washizu [15]) to overcome physical inconsistencies and to predict high order effects. Studying real problems, this is not feasible. There is the necessity of truncating the expansion of the primary mechanical variables, along the smallest dimensions of the structure domain, to a given order, which is generally done when formulating structure's theories. Furthermore, the more the terms in the kinematics, the more the complexity of the formulation and resolution of the problem is. The CUF represents a solution for these issues, describing the governing equations in a compact and unified form, allowing the formulation of 1D and 2D models (beam and plate models, respectively).

Let us consider a generic beam structure whose longitudinal axis, with respect to a Cartesian coordinate system, lays on the coordinate y , being its cross section defined in the xz -plane. The displacement field of one-dimensional models in CUF framework is described as a generic expansion of the generalized displacements (in the case of displacement-based theories) by arbitrary functions of the cross-sectional coordinates:

$$\mathbf{u}(x, y, z) = F_\tau(x, z)\mathbf{u}_\tau(y) \quad \tau = 1, 2, \dots, M, \quad (1)$$

where $\mathbf{u} = \{u_x, u_y, u_z\}$ is the vector of 3D displacements and $\mathbf{u}_\tau = \{u_{x\tau}, u_{y\tau}, u_{z\tau}\}$ is the vector of general displacements, M is the number of terms in the expansion, τ denotes summation and the functions $F_\tau(x, z)$ define the 1D model to be used. In fact, depending on the choice of $F_\tau(x, z)$ functions, different classes of beam theories can be implemented, such as Euler–Bernoulli or Timoshenko beam models and so forth.

In the framework of plate theories, by considering the mid-plane of the plate laying in the xy -plane, CUF can be formulated in an analogous manner (see [16]):

$$\mathbf{u}(x, y, z) = F_\tau(z)\mathbf{u}_\tau(x, y) \quad \tau = 1, 2, \dots, M. \quad (2)$$

In the equation above, the generalized displacements are function of the mid-plane coordinates of the plate and the expansion is conducted in the thickness direction z . Again, depending on the choice of the F_τ expanding functions,

various theories can be formulated, such as Kirchoff–Love or Reissner–Mindlin plate models and so forth. In this paper, only Lagrange expansions are considered, but other types of expansions based on the use of Taylor or Legendre polynomials can be conveniently employed as discussed in many previous works by Carrera et al. [8, 10, 14].

2.1 Lagrange Expansions

Lagrange expansions theories are based on the use Lagrange-type polynomials as generic functions over the cross section or along the thickness.

In the case of beam models, the cross section is divided into a number of local expansion sub-domains, whose polynomial degree depends on the type of Lagrange expansion employed. Four-nodes bilinear Q4, nine-nodes cubic Q9 and sixteen-nodes quartic Q16 polynomials can be used to formulate refined beam theories (see Carrera and Petrolo [17]). For example, the interpolation functions of a Q9 expansion are defined as

$$\begin{aligned}
 F_\tau &= \frac{1}{4}(\xi^2 + \xi \xi_\tau)(\zeta^2 + \zeta \zeta_\tau) \quad \tau = 1, 3, 5, 7 \\
 F_\tau &= \frac{1}{2}\zeta_\tau^2(\zeta^2 + \zeta \zeta_\tau)(1 - \xi^2) \\
 &\quad + \frac{1}{2}\xi_\tau^2(\xi^2 + \xi \xi_\tau)(1 - \zeta^2) \quad \tau = 2, 4, 6, 8 \\
 F_\tau &= (1 - \xi^2)(1 - \zeta^2) \quad \tau = 9,
 \end{aligned}
 \tag{3}$$

where ξ and ζ vary over the cross section between -1 and $+1$, and ξ_τ and ζ_τ represent the locations of the roots in the natural plane. The kinematic field of the single-Q9 beam theory is, therefore

$$\begin{aligned}
 u_x &= F_1(\xi, \zeta) u_{x_1} + F_2(\xi, \zeta) u_{x_2} + F_3(\xi, \zeta) u_{x_3} \\
 &\quad + \dots + F_9(\xi, \zeta) u_{x_9} \\
 u_y &= F_1(\xi, \zeta) u_{y_1} + F_2(\xi, \zeta) u_{y_2} + F_3(\xi, \zeta) u_{y_3} \\
 &\quad + \dots + F_9(\xi, \zeta) u_{y_9} \\
 u_z &= F_1(\xi, \zeta) u_{z_1} + F_2(\xi, \zeta) u_{z_2} + F_3(\xi, \zeta) u_{z_3} \\
 &\quad + \dots + F_9(\xi, \zeta) u_{z_9}.
 \end{aligned}
 \tag{4}$$

Refined beam models can be obtained by adopting higher order Lagrange polynomials or using a combination of Lagrange polynomials on multi-domain cross sections. More details about Lagrange-class beam models can be found in [17–20].

Plate theories based on Lagrange expansion are formulated by adopting 1D Lagrange polynomials as F_τ thickness functions up to the desired order p :

$$\begin{aligned}
 u_x &= F_1(\zeta) u_{x_1} + F_i(\zeta) u_{x_i} \\
 u_y &= F_1(\zeta) u_{y_1} + F_i(\zeta) u_{y_i}, \\
 u_z &= F_1(\zeta) u_{z_1} + F_i(\zeta) u_{z_i}
 \end{aligned}
 \tag{5}$$

where i denotes a summation and ranges from 2 to $p + 1$. In this way two-nodes linear B2, three-nodes parabolic B3 and four-nodes cubic B4 polynomials can be used.

Within the framework of 2D CUF theories, displacement fields like the one above have been used for the implementation of layerwise models for laminated structures (see, for example, [14, 21, 22]).

Lagrange polynomials have been extensively employed in the formulation of variable kinematics plate and shell theories in a unified framework by Kulikov and his co-workers. The readers are referred to the original papers for more details about 2D models based on Lagrange-type expansions, see, for example, [23, 24].

3 Finite-Element Formulation

The main advantage of CUF is that it allows to write the governing equations and the related finite-element arrays in a compact and unified manner, which is formally an invariant with respect to the F_τ functions. In the sections below, the mathematical derivation of the fundamental nucleus (the invariant) of the stiffness matrix in the case of CUF 1D and 2D models is provided in detail.

3.1 Geometrical Relations and Constitutive Equations

In this section, the same notation and reference system as defined in Sect. 2 are adopted. Let the 3D displacement vector be defined as

$$\mathbf{u}(x, y, z) = \begin{Bmatrix} u_x(x, y, z) \\ u_y(x, y, z) \\ u_z(x, y, z) \end{Bmatrix}.
 \tag{6}$$

According to classical elasticity, stress and strain tensors can be organized in six-term vectors with no lack of generality. They read, respectively:

$$\begin{aligned}
 \boldsymbol{\sigma}^T &= \{ \sigma_{yy} \ \sigma_{xx} \ \sigma_{zz} \ \sigma_{xz} \ \sigma_{yz} \ \sigma_{xy} \} \\
 \boldsymbol{\epsilon}^T &= \{ \epsilon_{yy} \ \epsilon_{xx} \ \epsilon_{zz} \ \gamma_{xz} \ \gamma_{yz} \ \gamma_{xy} \}.
 \end{aligned}
 \tag{7}$$

Regarding to this expression, the geometrical relations between strains and displacements with the compact vectorial notation can be defined as

$$\boldsymbol{\epsilon} = \mathbf{D} \mathbf{u},
 \tag{8}$$

where, in the case of small deformations and angles of rotations, \mathbf{D} is the following linear differential operator:

$$\mathbf{D} = \begin{bmatrix} 0 & \frac{\partial}{\partial y} & 0 \\ \frac{\partial}{\partial x} & 0 & 0 \\ 0 & 0 & \frac{\partial}{\partial z} \\ \frac{\partial}{\partial z} & 0 & \frac{\partial}{\partial x} \\ 0 & \frac{\partial}{\partial z} & \frac{\partial}{\partial y} \\ \frac{\partial}{\partial y} & \frac{\partial}{\partial x} & 0 \end{bmatrix}. \tag{9}$$

On the other hand, for isotropic materials the relation between stresses and strains is obtained through the well-known Hooke’s law:

$$\boldsymbol{\sigma} = \mathbf{C} \boldsymbol{\varepsilon}, \tag{10}$$

where \mathbf{C} is the isotropic stiffness matrix

$$\mathbf{C} = \begin{bmatrix} C_{22} & C_{21} & C_{23} & 0 & 0 & 0 \\ C_{21} & C_{11} & C_{13} & 0 & 0 & 0 \\ C_{23} & C_{13} & C_{33} & 0 & 0 & 0 \\ 0 & 0 & 0 & C_{55} & 0 & 0 \\ 0 & 0 & 0 & 0 & C_{44} & 0 \\ 0 & 0 & 0 & 0 & 0 & C_{66} \end{bmatrix}. \tag{11}$$

The coefficients of the stiffness matrix depend only on the Young’s modulus, E , and the Poisson ratio, ν , and in the case of isotropic materials, they are:

$$\begin{aligned} C_{11} = C_{22} = C_{33} &= \frac{(1 - \nu)E}{(1 + \nu)(1 - 2\nu)} \\ C_{21} = C_{13} = C_{23} &= \frac{\nu E}{(1 + \nu)(1 - 2\nu)} \\ C_{44} = C_{55} = C_{66} &= \frac{E}{2(1 + \nu)} \end{aligned} \tag{12}$$

3.2 Approximation of Displacements

In the case of 1D models, the discretization along the longitudinal axis of the beam is made by means of the finite-element method. The generalized displacements are in this way described as functions of the unknown nodal vector, $\mathbf{q}_{\tau i}$, and the 1D shape functions, $N_i(\eta)$:

$$\mathbf{u}_{\tau}(y) = N_i(\eta)\mathbf{q}_{\tau i}, \quad i = 1, 2, \dots, n_{elem}, \tag{13}$$

where n_{elem} is the number of nodes per element and the unknown nodal vector is defined as

$$\mathbf{q}_{\tau i} = \left\{ q_{u_{x\tau i}} \quad q_{u_{y\tau i}} \quad q_{u_{z\tau i}} \right\}^T. \tag{14}$$

Similarly, the FEM discretization of generalized displacements on the midsurface of the plate can be written as follows:

$$\mathbf{u}_{\tau}(x, y) = N_i(\xi, \eta)\mathbf{q}_{\tau i}, \quad i = 1, 2, \dots, n_{elem}, \tag{15}$$

where 2D shape functions $N_i(\xi, \eta)$ are employed.

Different sets of polynomials can be used to define FEM elements. Lagrange interpolating polynomials have been chosen in this work to generate both one-dimensional and two-dimensional elements. For the sake of brevity, their expression is not provided, but it can be found in the book by Carrera et al. [13], in which two-nodes (B2), three-nodes (B3) and four-nodes (B4) beam elements and four-nodes (Q4), nine-nodes (Q9) and 16-nodes (Q16) plate elements are described.

By combining the FEM approximation with the kinematic assumptions of the CUF, the 3D displacement field can be written as

$$\mathbf{u} = F_{\tau} N_i \mathbf{q}_{\tau i}, \tag{16}$$

where the functions F_{τ} and N_i are defined according to the type of element (beam or plate).

3.3 Node-Dependent Kinematic Approach

In Eq. 16, the shape functions N_i and the expanding functions F_{τ} are independent. Recently, Carrera et al. [13, 25, 26] introduced a coupling by relating the expanding functions F_{τ} to the shape functions N_i by means of the following formalism:

$$\mathbf{u} = F_{\tau}^i N_i \mathbf{q}_{\tau i}. \tag{17}$$

The difference of Eq. 17 from Eq. 16 is the additional superscript i of N_i , which is now an index also of the function F_{τ} . This definition introduces the dependency of the kinematic assumptions to the FE nodes, namely, the NDK.

As mentioned before, expanding functions with an increased order provide the chance to the better approximation of the structure responses. With NDK, the kinematic models can be refined locally on specific nodes which makes it easy to perform a local adaptable kinematic refinement with convenience. Different theories of structures will be blended naturally by the nodal shape functions within the element domain without any special coupling approaches. Meanwhile, no compatibility requirements for different nodal kinematics are needed.

The NDK technique can be applied to the efficient global–local modeling of structures. The kinematic model in the critical zone can be refined until the ideal accuracy is achieved while leaving the outlying area modeled with adequate lower order theories. Global–local FE model can be

constructed conveniently without changing the meshes, and the same set of mesh grids can be re-used to build a family of models for concurrent global–local analyzes. This approach has been used in the efficient modeling of laminated structures in both 1D [25, 26] and 2D [13, 17, 27] cases.

3.4 3D Modelling for Non-orthogonal Geometries

Classical beam and plate theories cannot be clearly employed in the modelling of beam with variable section or section not orthogonal to the axis, as well as plate with variable thickness or edges not orthogonal to the midsurface. In the framework of NDK approach, it is possible to extend the models of CUF to the modelling of this kind of geometries by incorporating the CUF kinematic assumption and the FEM discretization in a unique 3D approximation, as follows:

$$\mathbf{u} = (F_\tau^i N_i) \mathbf{q}_{\tau i} = L_{\tau i}(\xi, \eta, \zeta) \mathbf{q}_{\tau i}, \tag{18}$$

where ξ, η, ζ are the natural coordinates corresponding to x, y, z . In this expression, $L_{\tau i} = (F_\tau^i N_i)$ represents a non-conventional 3D shape function in which the order of expansion can be different along one of the spatial directions. Similarly, the virtual variation of displacements, that will be used in the derivation of governing equations below, can be approximated by

$$\delta \mathbf{u} = (F_s^j N_j) \delta \mathbf{q}_{s j} = L_{s j}(\xi, \eta, \zeta) \delta \mathbf{q}_{s j}, \tag{19}$$

where new summation indexes s and j have been introduced. Considering this formalism, the volume integrals involved in the governing equations will be not split in 1D and 2D integrals as usual, but the functions $(N_i F_\tau)$ and $(N_j F_s)$ will be handled as regular 3D shape functions; consequently, the Jacobian matrix relative to the transformation from natural coordinates ξ, η, ζ to global coordinates x, y, z will be computed in 3D form.

The results will demonstrate that this particular approach allow us to save degrees of freedom with respect to the use of meshes based on classical 3D finite elements. Indeed, conventional 3D elements employ the same order of expansion in the three spatial directions and this usually implies some limitations on the choice of the aspect ratio of the element by leading to a detrimental increase of the number of elements used.

3.5 Governing Equations

The governing equations are obtained via the principle of virtual displacements. This variational statement sets as a necessary condition for the equilibrium of a structure that

the virtual variation of the internal work has to be equal to the virtual variation of external work, or

$$\delta L_{int} + \delta L_{ine} = \delta L_{ext}. \tag{20}$$

The internal work is equivalent to the elastic strain energy:

$$\delta L_{int} = \int_V \delta \boldsymbol{\epsilon}^T \boldsymbol{\sigma} dV, \tag{21}$$

where V stands for the volume of the domain. By adopting the geometrical relation [Eq. (8)], the constitutive law [Eq. (10)], the CUF kinematic field [Eq. (1)] and the FEM discretization [Eq. (13)], the internal work can be rewritten as

$$\delta L_{int} = \delta \mathbf{q}_{\tau i}^T \mathbf{K}^{\tau s i j} \mathbf{q}_{s j}, \tag{22}$$

where $\mathbf{K}^{\tau s i j}$ is the 3×3 fundamental nucleus of the stiffness matrix.

The inertial work can be written as

$$\delta L_{ine} = \int_V \delta \mathbf{u}^T \boldsymbol{\rho} \ddot{\mathbf{u}} dV. \tag{23}$$

By adopting the CUF kinematic field and the FEM discretization (Eqs. (18) and (19)), it becomes:

$$\delta L_{ine} = \delta \mathbf{q}_{\tau i}^T \mathbf{M}^{\tau s i j} \ddot{\mathbf{q}}_{s j}, \tag{24}$$

where $\mathbf{M}^{\tau s i j}$ is the 3×3 fundamental nucleus of the mass matrix.

The external work can be written as

$$\delta L_{ext} = \int_V \delta \mathbf{u}^T \mathbf{g} dV. \tag{25}$$

Following the same steps done for the internal work, it is possible to write also the external work in terms of nodal vector $q_{\tau i}$ as

$$\delta L_{ext} = \delta \mathbf{q}_{\tau i}^T \mathbf{P}^{\tau i}, \tag{26}$$

where $\mathbf{P}^{\tau i}$ is the load vector in terms of shape functions N_i and expanding functions F_τ .

It should be noted that the formal expressions of the components of the fundamental nuclei are independent on the choice of the expanding functions F_τ , which determine the theory of structure, and shape functions N_i , which determine the numerical accuracy of the FEM approximation. This means that any beam or plate element can be automatically formulated by appropriately expanding the fundamental nuclei according to the indexes $\tau, s, i,$ and j . For more details about the expressions of fundamental nuclei of stiffness, mass and load matrices, the reader can refer to the work [28].

In this paper, linear, quadratic and cubic Lagrange-type shape functions are used for both F_τ and N_i functions.

Note that the acronyms B2 (linear), B3 (quadratic) and B4 (cubic) are used both for the 1D discretization of the axis in beam models and for the approximation through the thickness in plate models; as well as the acronyms Q4 (linear), Q9 (quadratic) and Q16 (cubic) are used both for the 2D approximation of the cross section in beam models and for the discretization of the midsurface in plate models. According to these characteristics, the expansion order is set as a free input of the model that determines the number of unknowns to be solved. At the same time, the kinematic field can be enriched in particular zones of interest through the definition of multi-domain cross sections.

4 Numerical Results

In this section, some benchmark problems are considered for assessing the robustness of the proposed Adaptive Elements based on CUF. First, a set of problems involving a homogeneous and isotropic plate is used for assessing the element's performance, shown in Sect. 4.1: the displacement sensitivity concerning distorted element shapes and the free-vibration analysis are considered. The influence of the boundary conditions is also addressed.

Then, static and modal analyses are performed on a plate with distorted elements. The distorted mesh was created in a random way starting from the regular pattern: the new positions of nodes are obtained using a function which generates a random scalar drawn from the normal or Gaussian distribution having a mean equal to the previous position and different standard deviations.

For all the listed problems, both four-node and nine-node elements are considered.

4.1 Patch Test

This standard test is classically used to investigate the mesh distortion sensitivity in plate bending problems. The in-plane dimensions of the square plate considered are $100 \times 100 \text{ m}^2$, while the thickness is 5 m. The boundary conditions applied are: clamped–clamped (CC), all edges are fixed; simply supported (SS), all edges have no displacement in the thickness direction and the direction parallel to the edge. The load is expressed as a concentrated force at the centre of the top surface equal to $F = 4 \text{ N}$. The material considered is isotropic with the following properties: $E = 10.92 \text{ Pa}$, $\nu = 0.30$ and $\rho = 1 \text{ kg/m}^3$. The starting meshes are a 4×4 Q4 elements and a 4×4 Q9 elements in the plane, with B3 approximation along the thickness in both cases.

Due to the symmetry of the problem, with symmetric geometry and symmetric boundary conditions, a quarter of the plate is considered to simplify the analysis: the full plate is divided into four equal sub-plates and the study is

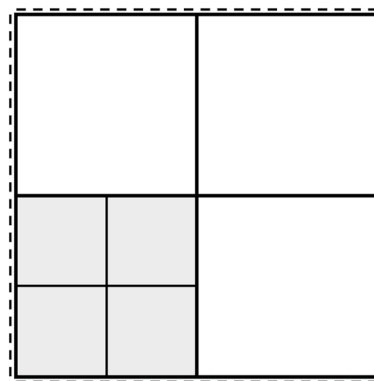


Fig. 1 Isotropic plate with transversal concentrated load in the center point. Only a quarter of the plate is meshed with 2×2 elements

conducted only on one of them, as shown in Fig. 1. In particular, the bottom-left quarter is chosen and the following boundary conditions are applied, considering as u , v and w the displacements along x , y and z , respectively: bottom and left edges are fixed or simply-supported, on the top edge $v = 0$, on the right edge $u = 0$ and on the top-right corner a force of $F = 1 \text{ N}$ is applied.

4.2 Mesh Distortion Sensitivity

The resulting mesh of the plate quarter is 2×2 based on Q4 or Q9 elements with B3 discretization along the thickness, see Fig. 2.

Note that from now on, some beam elements are introduced in the mesh to obtain distorted elements with different numbers of nodes along the edges. Then, three different configurations are analyzed:

- **2xQ4 1xB2:** in this configuration, the previous two elements at the top are substituted by a single 1D element with 2 nodes, having a Q9 approximation on the cross section;
- **2xQ4 1xB3:** as in the previous case, the two elements at the top are substituted by a single 1D element but having 3 nodes along the axis, where the cross section is expressed as a Q9 element;
- **2xQ4 1xQ9:** the number of nodes is identical with respect to the previous case, but the discretization of the two elements at the top is different, accounting for a single Q9 element having a B3 discretization along the thickness.

In Figs. 3 and 4, it is possible to visualize the described configurations: the black dots are the nodes used during the implementation, while the white dots represent the nodes added considering the thickness and the cross section of the plate and the beam elements, respectively. A color code

Fig. 2 Quarter plate—original mesh

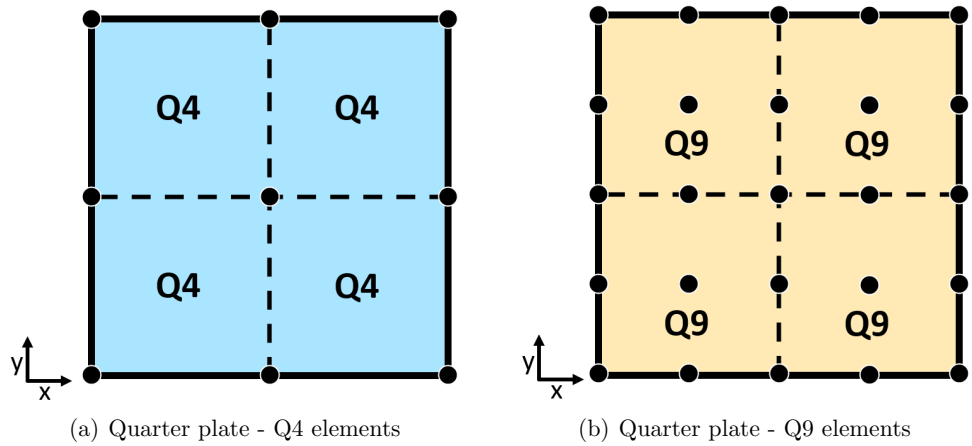


Fig. 3 Quarter plate—2xQ4 1xB2

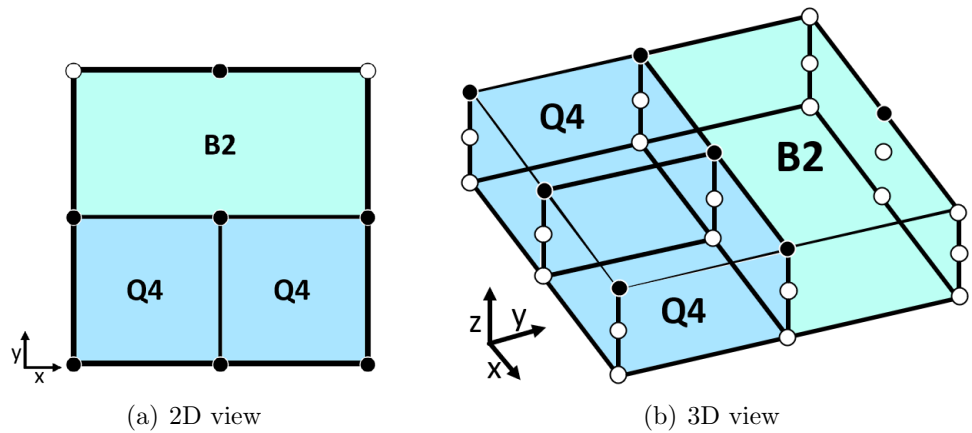
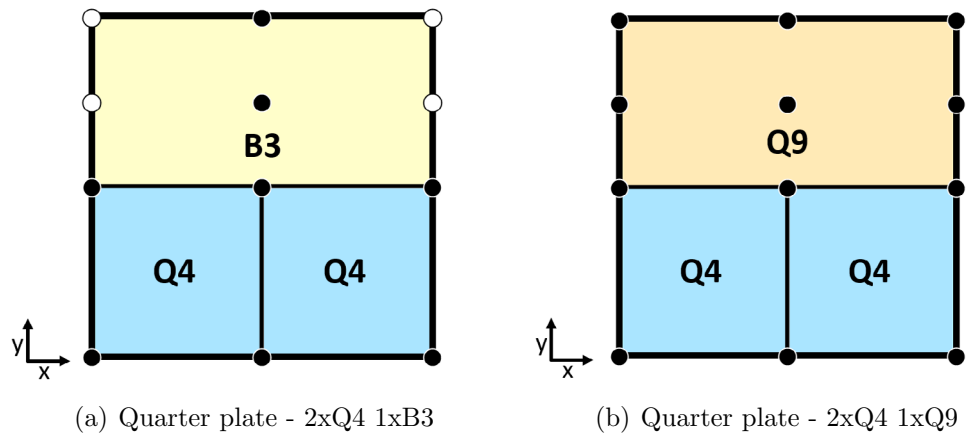


Fig. 4 Quarter plate—two different configurations



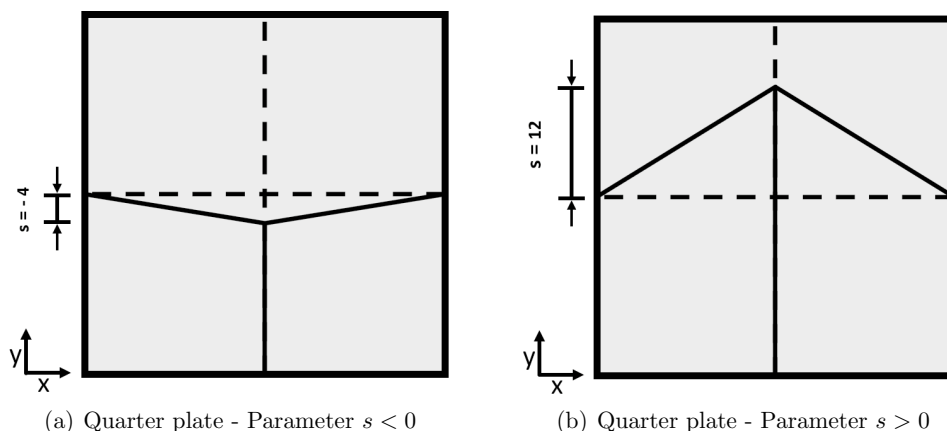
is introduced for the different elements: the B2 element is colored heavenly, the B3 element is colored yellow, the Q4 element is colored light blue and the Q9 element is colored orange.

The emphasis now will be focused on the beam elements and on the possibility to freely move its nodes thanks to the

3D integration of its approximation function, as discussed in Sect. 3.4.

The mesh distortion is characterized by the parameter $s \in \{-12, -10, -6, 0, 6, 10, 12\}$, which defines the coordinates of the central node of the plate quarter. Note that the parameter s can have negative and positive values both: this is not common in literature and, particularly in this work, it is used to control the property of the element: in

Fig. 5 Quarter plate—mesh distortion defined by parameter s



fact, as shown in Fig. 5, if the parameter s is negative, the considered element is convex; if the parameter s is positive, the element becomes non-convex. The y -coordinate of the mid-node changes according to s : defining a as the length of the quarter plate, the coordinate varies as $y = (a/2) + s$, where in Fig. 5a $s = -4$, so the coordinate is $y = (a/2) - 4$; in Fig. 5b $s = 12$, so the coordinate is $y = (a/2) + 12$.

4.2.1 Static and Modal Analysis

The three different configurations are used to perform a static and modal analysis, as done in Ref. [29]. Regarding the static analysis, the results are computed in terms of transverse displacement $U_z = u_z(a, a, 0)$ (the center point on the midsurface of the entire plate) for the distorted mesh and it is normalized with respect to the reference value U_z^0 calculated for the regular mesh ($s = 0$). The values of U_z^0 for the different meshes are compared with the 3D solution computed in Nastran for validation purposes. One can note that the 2x2Q9 solution is the most accurate with the highest number of degrees of freedom, the 2x2Q4 is the least accurate and the other solutions are in the middle according to their related degree of approximation. The meshes 2xQ4 1xQ9 and 2xQ4 1xB3 are very similar and they are compared to highlight that their solution are exactly the same, although the first uses a plate element (Q9) and the other one a beam element (B3). Moreover, one can see that the 2xQ4 1xB2 solution is more accurate than the 2x2Q4 one, although the number of degrees of freedom is the same: this is due to the use of quadratic approximation over the cross section of the B2 beam element. We can conclude that the present adaptive elements permit to increase the accuracy with respect to regular meshes with the same degrees of freedom (Table 1).

In addition, the results computed by varying the parameter s are reported in Figs. 6 and 7, where also different boundary conditions are considered (CC and SS, respectively). In both cases, these graphics demonstrate that the

Table 1 Tip displacement

	Configuration	U_z^0	DOFs
CC	4xQ4	0.2784	81
	2xQ4 1xB2	0.3276	81
	2xQ4 1xB3	0.4883	108
	2xQ4 1xQ9	0.4883	108
	4xQ9	1.5804	225
	Nastran®	1.6612	513
SS	4xQ4	0.7542	81
	2xQ4 1xB2	1.0207	81
	2xQ4 1xB3	2.4678	108
	2xQ4 1xQ9	2.4678	108
	4xQ9	3.5733	225
	Nastran®	3.6003	513

sensitivity to the distortion of the mixed meshes with beam elements is comparable to the regular meshes (2x2Q4 and 2x2Q9). The behaviors of 2xQ4 1xQ9 and 2xQ4 1xB3 meshes are again very similar; moreover, one can note that the use of B2 beam element in the mesh 2xQ4 1xB2 does not compromise the accuracy of the results when the mesh is distorted, although it permits to differentiate the number of nodes along the edges of the element (see Fig. 3b) by reducing the total number of the nodes in the element.

Finally, a free-vibration analysis is performed considering the different values of the parameter s . The results are shown in Figs. 8 and 9 in terms of natural frequencies associated with the first 16 modes: in this analysis, no boundary conditions are applied, hence only the non-null modes are reported. It is evident that the conclusions drawn before are confirmed: the solutions of the mixed meshes lie between the regular meshes, 2x2Q4 and 2x2Q9; the mixed meshes 2xQ4 1xQ9 and 2xQ4 1xB3 provide the same results, except in the case of $s = -12$ for SS boundary conditions; the solution 2xQ4 1xB2 provide lower natural frequencies than the 2x2Q4 regular mesh, so one can suppose it is more accurate.

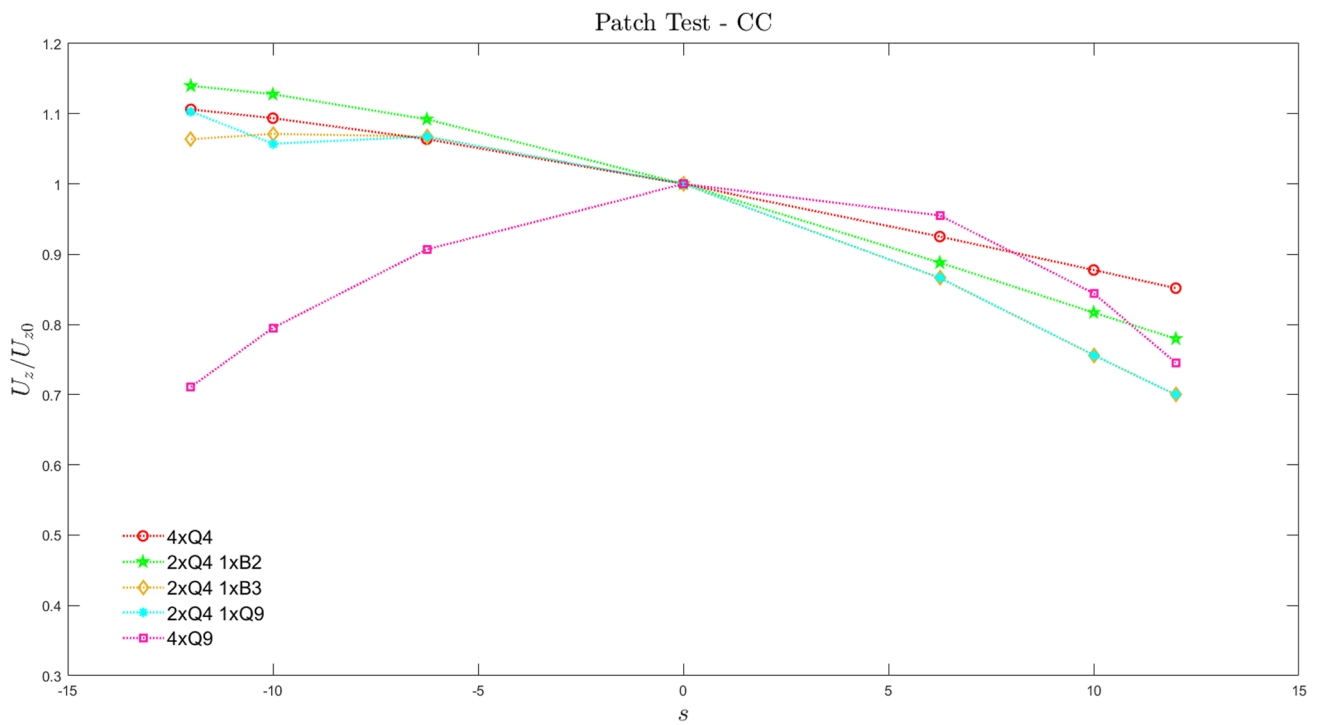


Fig. 6 Variation of the ratio U_z/U_z^0 for CC quarter plate

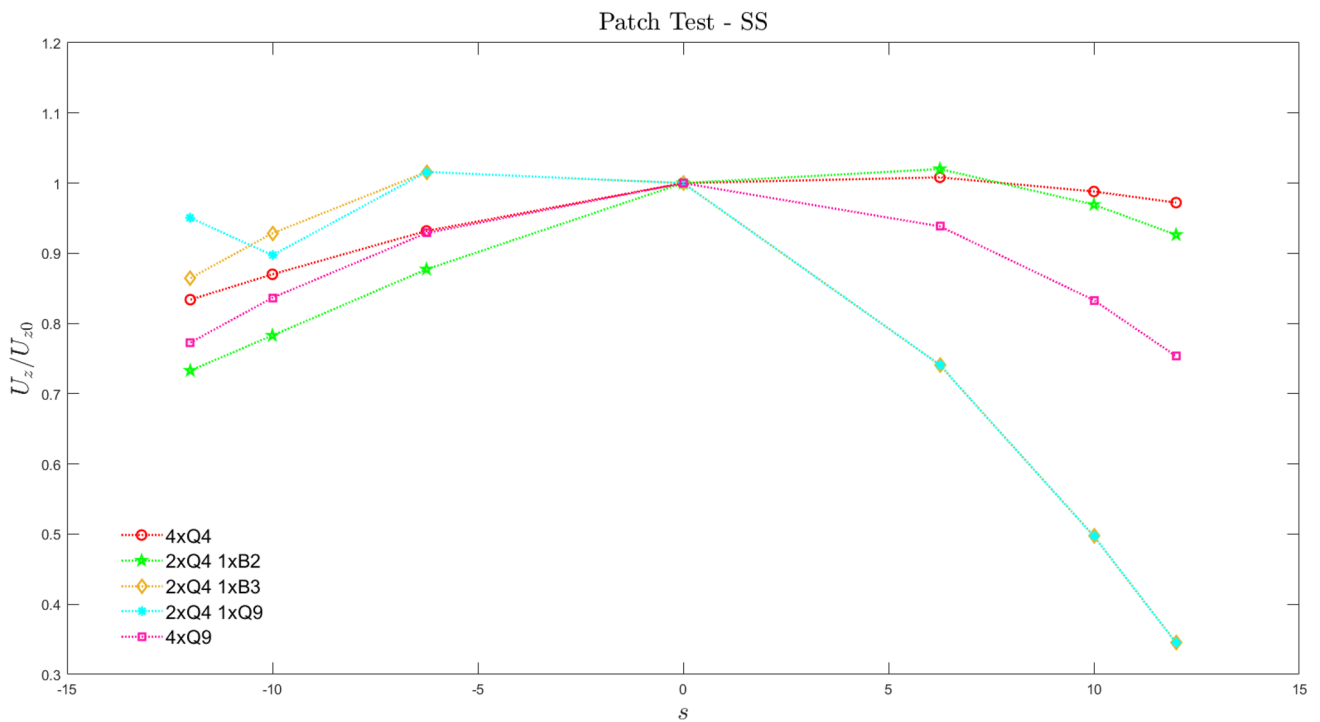


Fig. 7 Variation of the ratio U_z/U_z^0 for SS quarter plate

Modal analysis - CC

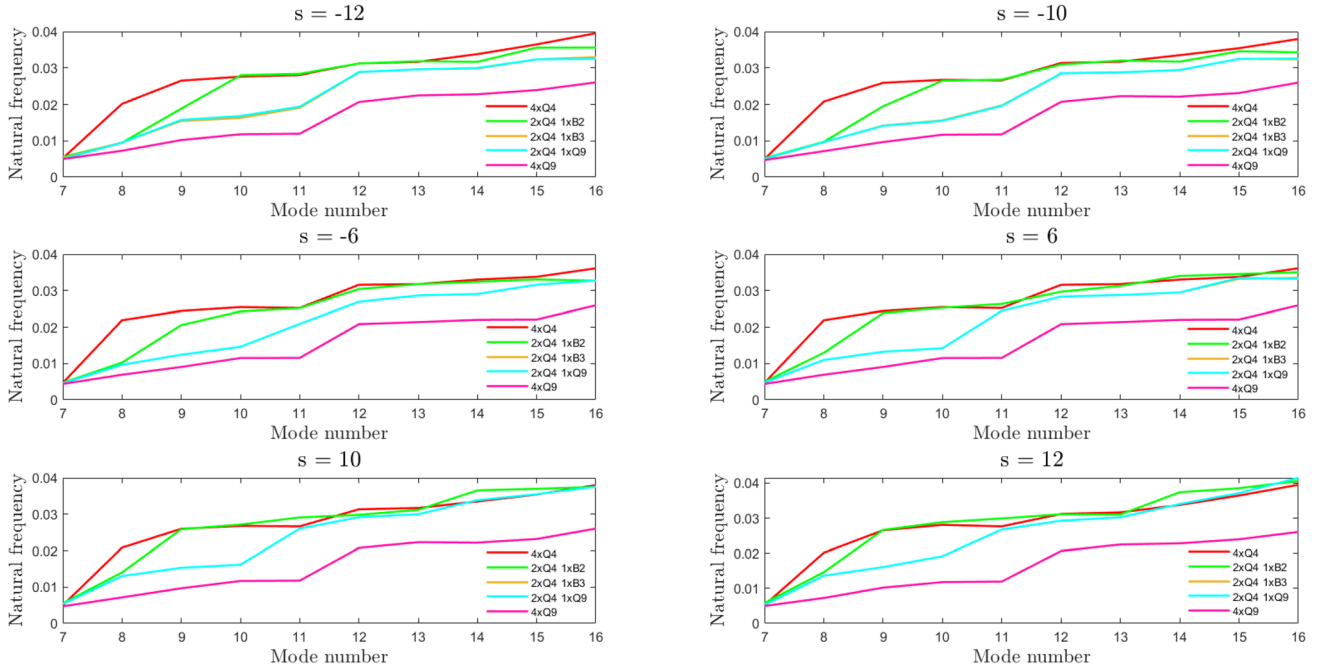


Fig. 8 Quarter plate CC—modal analysis for different values of s

Modal analysis - SS

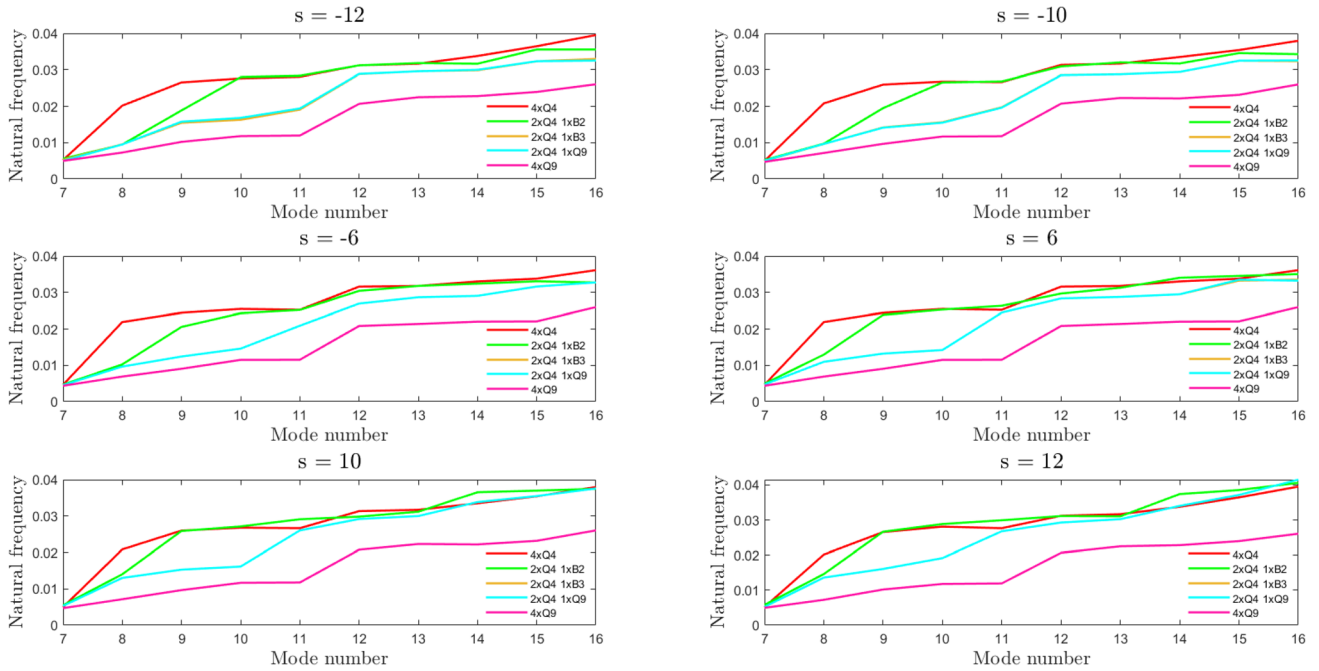
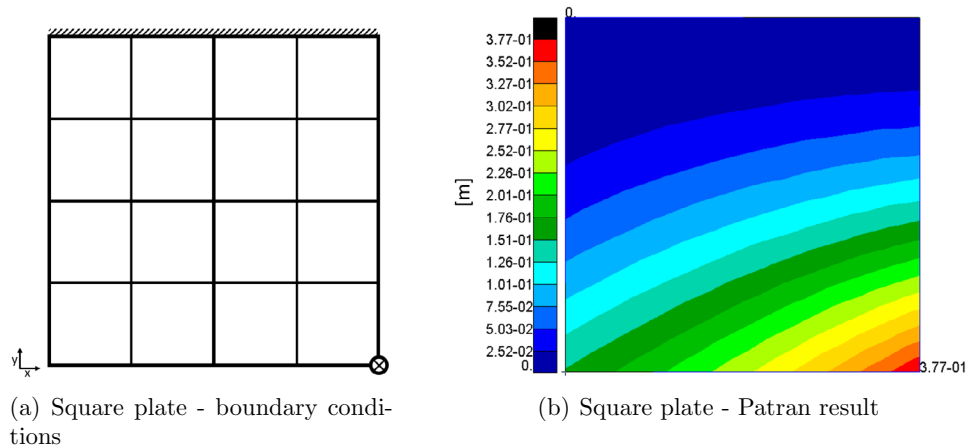


Fig. 9 Quarter plate SS—modal analysis for different values of s

Fig. 10 Square plate—regular mesh



4.3 Square Plate with Distorted Mesh

A full square plate is now considered to perform the static and modal analysis. The in-plane dimensions of the plate are $100 \times 100 \text{ m}^2$, while the thickness is 10 m . The boundary condition applied is a clamped edge (the top edge, as illustrated in Fig. 10a) and the load is expressed as a concentrated force at the right-bottom corner equal to $F = 5 \times 10^8 \text{ N}$, again represented in Fig. 10a as a crossed circle. The material considered is isotropic with the following properties: $E = 70 \text{ GPa}$, $\nu = 0.33$ and $\rho = 2.81 \times 10^3 \text{ kg/m}^3$. Note that a reference problem is analyzed with the commercial software Nastran® and illustrated in Fig. 10b. The starting meshes

are a 4×4 Q4 elements in the plane with B3 approximation along the thickness (DOFs = 225), and a 4×4 Q9 elements in the plane with B3 approximation again along the thickness (DOFs = 729).

Starting from these regular meshes, the elements are gradually distorted to demonstrate the capabilities of the presented adaptive elements. The nodes coordinates of some elements are varied in a random way, considering a Gaussian distribution having the mean equal to the original coordinate and the standard deviation increasing little by little. Stating that x_0 is the original coordinate of a node, σ_{dev} the standard deviation and μ the mean value, the new coordinates are obtained as follow: $x_0 = x_0 + \sigma_{\text{dev}} \cdot \text{randn}(\mu)$,

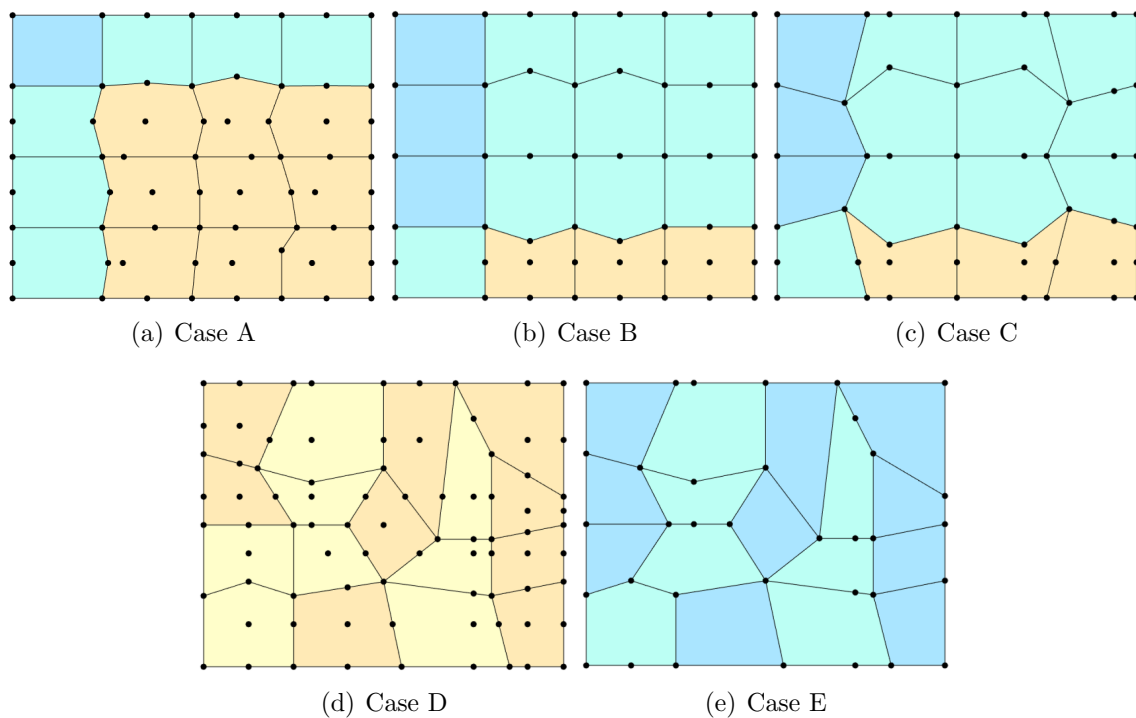


Fig. 11 Square plate—distorted meshes

where the Matlab[®] function `randn` returns pseudorandom values drawn from the standard normal distribution, $\mu = 1$ and the standard deviation varies in a range equal to $\sigma_{\text{dev}} \in \{1, 2, 3, 5\}$.

Moreover, in other examples, the nodes are moved intentionally to obtain specific shapes (for instance, a pentagon, which is a benchmark example for the virtual elements [3, 5, 30]). As a final example, a complete non-regular distorted mesh is considered. For all of these cases, a combination of plate and beam elements is exploited.

The previous meshes are reported in Fig. 11, where:

- Case A: in Fig. 11a Mesh 9xQ9 1xQ4 6xB2 (DOFs = 387)—the mesh is obtained using a standard deviation equal to $\sigma_{\text{dev}} = 3$;
- Case B: in Fig. 11b Mesh 3xQ9 3xQ4 10xB2 (DOFs = 330)—the mesh is obtained creating some pentagon elements;
- Case C: in Fig. 11c Mesh 3xQ9 3xQ4 10xB2 v2 (DOFs = 330)—an upgraded version of the previous mesh is obtained to highlight the presence of pentagon elements, leading to a more distorted mesh with the same number of DOFs;
- Case D: in Fig. 11d Mesh 9xQ9 8xB3 (DOFs = 765)—a complete distorted mesh is obtained and modelled using high order accuracy in the approximation of the kinematics (quadratic interpolation);

- Case E: in Fig. 11e Mesh 10xQ4 7xB2 (DOFs = 315)—a similar mesh to the previous one is considered, using a lower order accuracy of the kinematics approximation (linear interpolation), to investigate if it is possible to obtain comparable results with fewer degrees of freedom.

4.3.1 Static and Modal Analysis

The different meshes are investigated by performing static analysis and the results are reported in terms of displacements along the bottom free edge. In particular, in Fig. 12, the displacement magnitude is shown for the different meshes introduced above. Each mesh is analyzed and compared with the family of curves related to the Q4 and Q9 regular meshes. In particular, we consider: case A in which there is almost a balance between elements with high order accuracy (Q9) and elements with a lower order of accuracy (Q4, B2); case B in which the predominant elements are similar to the Q4 regular mesh; case C that is similar to the previous case, with the difference that now the pentagons are immersed in a more distorted mesh; cases D and E that, due to the severe distortion of the elements, tend to match the reference solutions related to Q9 distorted mesh with $\sigma_{\text{dev}} = 3$ for the first case and related to Q4 distorted mesh with $\sigma_{\text{dev}} = 5$ for the second case. In conclusion, it is evident that the results of the distorted meshes lie between the two reference curves of Q4 and Q9 regular meshes, with

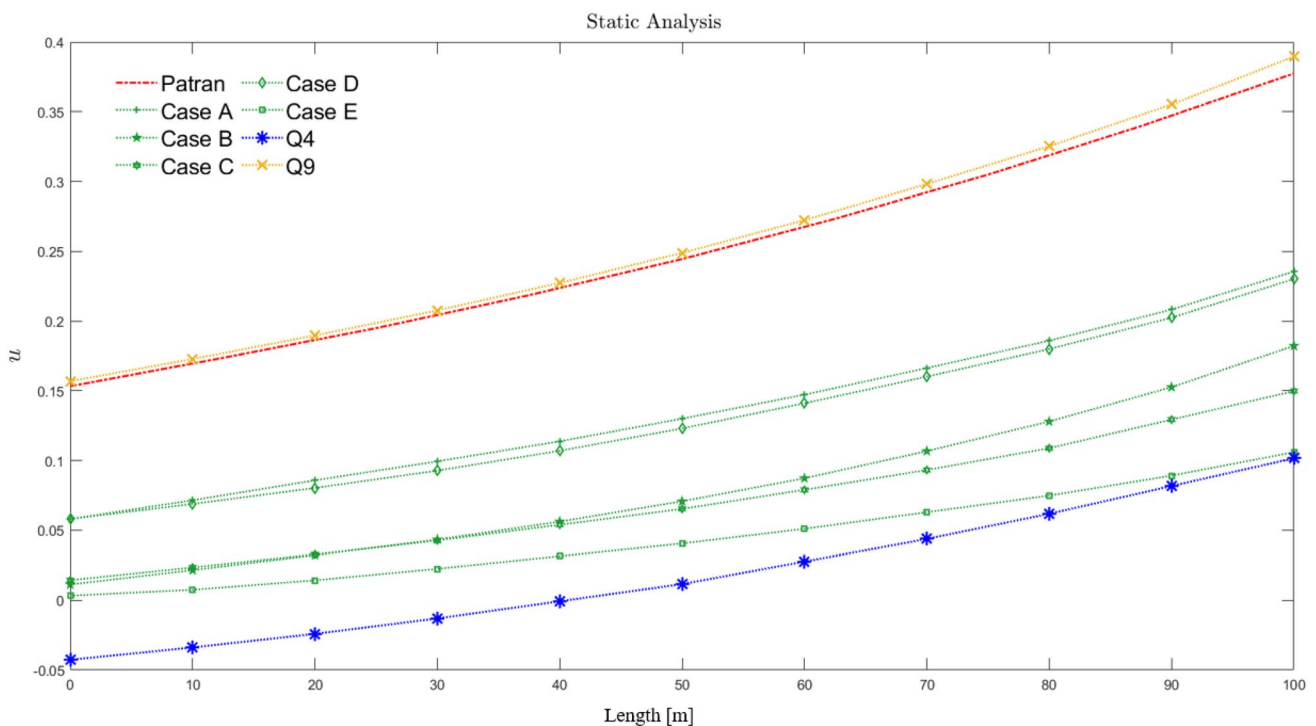


Fig. 12 Square plate—static analysis

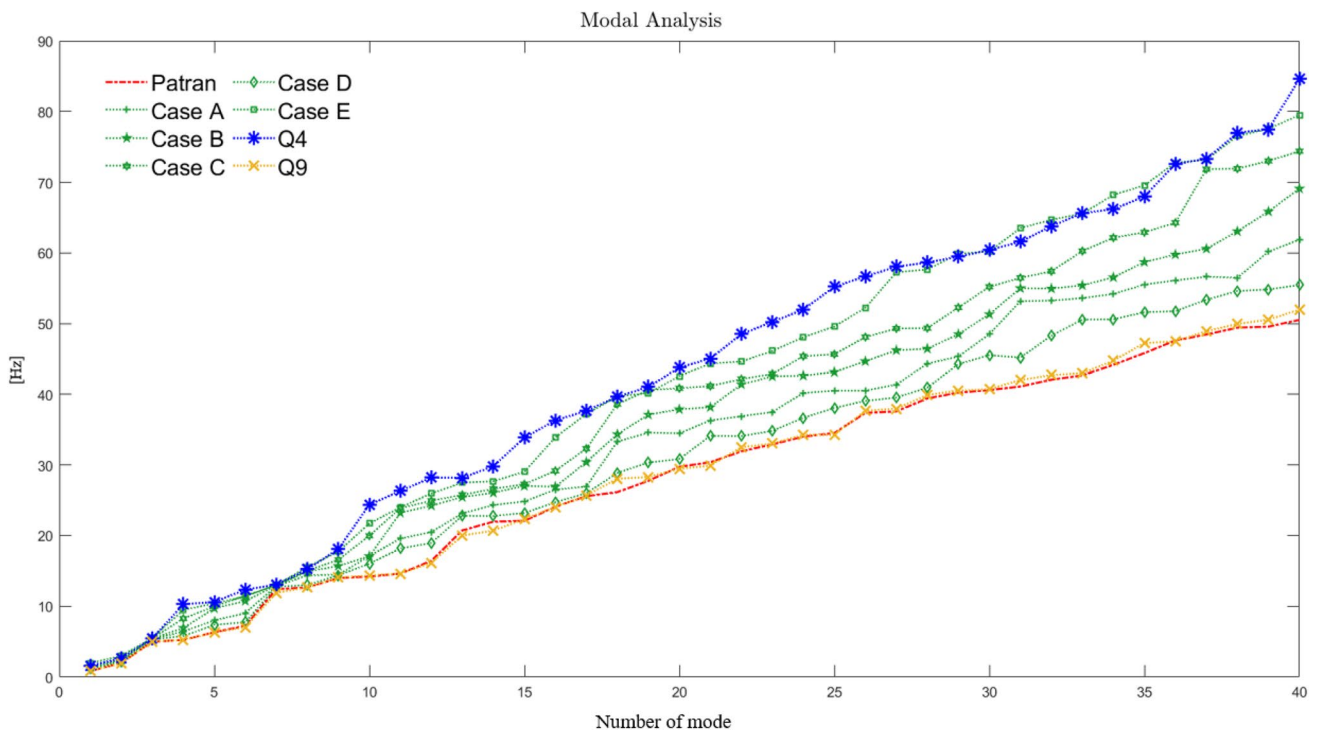


Fig. 13 Square plate—modal analysis

increasing accuracy according to the related number degrees of freedom.

In a similar way to the static analysis, also for the modal investigation the frequencies are compared with respect to the solutions of the Q4 and Q9 regular meshes, as shown in Fig. 13. Note that the frequencies of the distorted meshes are perfectly bounded by those of the regular meshes, in particular the case D is very close to the full Q9 solution.

5 Conclusions

In this paper, the assessment of adaptive elements based on the CUF with respect to distorted mesh has been proposed. In the framework of CUF, which is an advanced tool that enables to formulate theories of structure in a unified manner, the NDK approach was exploited along with a 3D modelling approach. A kinematic refinement on some nodes is possible by allowing to choose different expansions through the same element. This aspect represents a key point to reduce the number of nodes inside the element and, consequentially, the computational cost by keeping the same accuracy.

When dealing with meshing technique, using the FEM, the main issue is the difficulty of approximate the physical domain with elements which must be triangular or

quadrilateral in 2D and tetrahedral or hexahedral in 3D trying to contain, at the same time, the number of elements for computational cost reasons. The proposed adaptive elements can overcome these problems, offering a convenient solution.

The capabilities of these elements are already investigated in other works, see [28, 31]. This work aims to demonstrate that different polygons and polyhedra can be constructed using the adaptive elements, with a relatively low number of degrees of freedom, and to assess their performances when severe mesh distortions arise. Static and modal analyses are conducted, giving results in terms of displacements and natural frequencies. The outcomes are presented for distinct distorted meshes, combining elements with different kinematic approximations. The standard tests and the example problems analyzed prove that convenient distorted mesh (from a computational point of view) can be accomplished and the effect of distortion is comparable to classical elements.

Further studies shall concern the application of the adaptive elements to the analysis of shell structures, relying on the formulation of these elements in curvilinear coordinates, according to the recent author's work [32].

Funding Open access funding provided by Politecnico di Bari within the CRUI-CARE Agreement.

Open Access This article is licensed under a Creative Commons Attribution 4.0 International License, which permits use, sharing, adaptation, distribution and reproduction in any medium or format, as long as you give appropriate credit to the original author(s) and the source, provide a link to the Creative Commons licence, and indicate if changes were made. The images or other third party material in this article are included in the article's Creative Commons licence, unless indicated otherwise in a credit line to the material. If material is not included in the article's Creative Commons licence and your intended use is not permitted by statutory regulation or exceeds the permitted use, you will need to obtain permission directly from the copyright holder. To view a copy of this licence, visit <http://creativecommons.org/licenses/by/4.0/>.

References

- Bathe, K.-J.: Finite element method. In: Wiley Encyclopedia of Computer Science and Engineering, pp. 1–12 (2007). <https://doi.org/10.1002/9780470050118.ecse159>
- Sorgente, T., Prada, D., Cabiddu, D., Biasotti, S., Patané, G., Pennacchio, M., Bertoluzza, S., Manzini, G., Spagnuolo, M.: Vem and the mesh. arXiv preprint [arXiv:2103.01614](https://arxiv.org/abs/2103.01614) (2021)
- Chi, H., Beirão Da Veiga, L., Paulino, G.: Some basic formulations of the virtual element method (vem) for finite deformations. *Comput. Methods Appl. Mech. Eng.* **318**, 148–192 (2017)
- da Veiga, L., Brezzi, F., Marini, L.D., Russo, A.: The hitchhiker's guide to the virtual element method. *Math. Models Methods Appl. Sci.* **24**(08), 1541–1573 (2014)
- van Huyssteen, D., Reddy, B.D.: A virtual element method for isotropic hyperelasticity. *Comput. Methods Appl. Mech. Eng.* **367**, 113134 (2020)
- Yaw, L.L.: Introduction to the virtual element method for 2d elasticity (2021). <https://doi.org/10.48550/arXiv.2301.11928>
- Carrera, E., Zappino, E.: One-dimensional finite element formulation with node-dependent kinematics. *Comput. Struct.* **192**, 114–125 (2017)
- Carrera, E., Pagani, A., Valvano, S.: Multilayered plate elements accounting for refined theories and node-dependent kinematics. *Compos. B Eng.* **114**, 189–210 (2017)
- Carrera, E., Zappino, E., Li, G.: Finite element models with node-dependent kinematics for the analysis of composite beam structures. *Compos. B Eng.* **132**(Supplement C), 35–48 (2018)
- Li, G., Carrera, E., Cinefra, M., de Miguel, A.G., Pagani, A., Zappino, E.: An adaptable refinement approach for shell finite element models based on node-dependent kinematics. *Compos. B Eng.* **210**, 1–19 (2019)
- Moleiro, F., Carrera, E., Zappino, E., Li, G., Cinefra, M.: Layerwise mixed elements with node-dependent kinematics for global-local stress analysis of multilayered plates using high-order legendre expansions. *Comput. Methods Appl. Mech. Eng.* **359**, 112764 (2020)
- Zappino, E., Li, G., Pagani, A., Carrera, E.: Global-local analysis of laminated plates by node-dependent kinematic finite elements with variable esl/lw capabilities. *Compos. Struct.* **172**, 1–14 (2017)
- Petrolo, M., Carrera, E., Giunta, G.: *Beam Structures: Classical and Advanced Theories*. Wiley, New York (2011)
- Carrera, E., Cinefra, M., Petrolo, M., Zappino, E.: *Finite Element Analysis of Structures through Unified Formulation*. Wiley, New York (2014)
- Washizu, K.: *Variational Methods in Elasticity and Plasticity*. Elsevier Science & Technology, Amsterdam (1974)
- Carrera, E.: Theories and finite elements for multilayered plates and shells: a unified compact formulation with numerical assessment and benchmarking. *Arch. Comput. Methods Eng.* **10**(3), 216–296 (2003)
- Carrera, E., Petrolo, M.: Refined beam elements with only displacement variables and plate/shell capabilities. *Meccanica* **47**(3), 537–556 (2012)
- Carrera, E., Pagani, A., Petrolo, M.: Component-wise method applied to vibration of wing structures. *J. Appl. Mech.* **80**(4), art. no. 041012, 1–15 (2013)
- Carrera, E., Pagani, A.: Free vibration analysis of civil engineering structures by component-wise models. *J. Sound Vib.* **333**(19), 4597–4620 (2014)
- Carrera, E., Pagani, A., Petrolo, M., Zappino, E.: Recent developments on refined theories for beams with applications. *Mech. Eng. Rev.* **2**(2), 14–00298 (2015)
- Cinefra, M., Valvano, S., Carrera, E.: A layer-wise MITC9 finite element for the free-vibration analysis of plates with piezopatches. *Int. J. Smart Nano Mater.* **6**(2), 85–104 (2015)
- Pagani, A., Valvano, S., Carrera, E.: Analysis of laminated composites and sandwich structures by variable-kinematic MITC9 plate elements. *J. Sandwich Struct. Mater.* **20**(1), 4–41 (2018). <https://doi.org/10.1177/1099636216650988>
- Kulikov, G.M., Mamontov, A.A., Plotnikova, S.V., Mamontov, S.A.: Exact geometry solid-shell element based on a sampling surfaces technique for 3d stress analysis of doubly-curved composite shells. *Curved Layered Struct.* **3**(1) (2016). <https://doi.org/10.1515/cls-2016-0001>
- Kulikov, G.M., Plotnikova, S.V.: A method of solving three-dimensional problems of elasticity for laminated composite plates. *Mech. Compos. Mater.* **48**(1), 15–26 (2012)
- Carrera, E., Giunta, G.: Refined beam theories based on Carrera's unified formulation. *Int. J. Appl. Mech.* **2**(1), 117–143 (2010)
- Carrera, E., Petrolo, M., Zappino, E.: Performance of cuf approach to analyze the structural behavior of slender bodies. *J. Struct. Eng.* **138**(2), 285–297 (2012)
- Carrera, E., Pagani, A.: Analysis of reinforced and thin-walled structures by multi-line refined 1D/beam models. *Int. J. Mech. Sci.* **75**, 278–287 (2013)
- Cinefra, M.: Non-conventional 1d and 2d finite elements based on cuf for the analysis of non-orthogonal geometries. *Eur. J. Mech. A Solids* **88**, 104273 (2021)
- Cinefra, M., D'Ottavio, M., Polit, O., Carrera, E.: Assessment of mitc plate elements based on cuf with respect to distorted meshes. *Compos. Struct.* **238**, 111962 (2020)
- Yaw, L.L.: Introduction to the virtual element method for 2d elasticity. arXiv preprint [arXiv:2301.11928](https://arxiv.org/abs/2301.11928) (2022)
- Cinefra, M., Rubino, A.: Adaptive mesh using non-conventional 1d and 2d finite elements based on cuf. *Mech. Adv. Mater. Struct.* **30**(3), 1–11 (2022). <https://doi.org/10.1080/15376494.2022.2126039>
- Cinefra, M.: Formulation of 3d finite elements using curvilinear coordinates. *Mech. Adv. Mater. Struct.* (2020). <https://doi.org/10.1080/15376494.2020.1799122>

Publisher's Note Springer Nature remains neutral with regard to jurisdictional claims in published maps and institutional affiliations.